

Supporting Information for:
Design and room-temperature operation of GaAs/AlGaAs
multi-quantum well nanowire lasers

I.	Design of MQW nanowire laser	1
	a. Modelling cavity losses	1
	i. Intrinsic loss	2
	ii. Mirror loss	3
	iii. Net modal loss	3
	b. Modelling modal gain	5
	i. Material gain	5
	ii. Mode confinement factor	6
	iii. Modal gain in a MQW nanowire laser	8
	iv. Optimum number of QWs	9
II.	Growth and optical characterization	11
	a. Growth of MQW nanowire heterostructure	11
	b. Structural characterization of nanowires	11
	i. Cross-section TEM analysis	12
	c. Photoluminescence measurements	13
III.	Laser characterization	15
	a. Nanowire laser dimensions	15
	b. Lasing spectra	15
	c. Mode confinement factor and group index	16
	d. Polarization analysis	17
	e. Rate Equation analysis	18
	i. Comparison between bulk and MQW nanowire lasers	19
	ii. Comparison with other reported III-V semiconductor nanowire lasers	21
IV.	References	23

I. Design of MQW nanowire laser

In this manuscript we present the design of a nanowire laser with coaxial GaAs/AlGaAs multi-quantum well (MQW) active regions. The heterostructure is illustrated in the schematic in Fig. S1 and consists of a GaAs core surrounded by an AlGaAs shell, coaxial GaAs/AlGaAs MQW shells and a thin GaAs cap. The nanowire has a hexagonal cross-section and is lying horizontally on a SiO₂ substrate. For the design, we have assumed that the GaAs MQWs are of equal thickness t_w and are uniformly separated by AlGaAs barriers of thickness t_b . The Al concentration in all AlGaAs layers in our nanowires is 42%. Since the Al concentration is fixed, the quantum confined energy levels at a given temperature are mainly determined by t_w . Therefore, t_w determines the peak emission wavelength λ_0 from the QWs and the wavelength at which laser cavity is to be designed. Here we investigate the design for MQW nanowire laser with $t_w = 2, 4$ and 6 nm, corresponding to room-temperature emission wavelengths ($E_{\text{qw}}^1 \rightarrow \text{HH}_{\text{qw}}^1$) $\lambda_0 = 730, 800, 830$ nm.

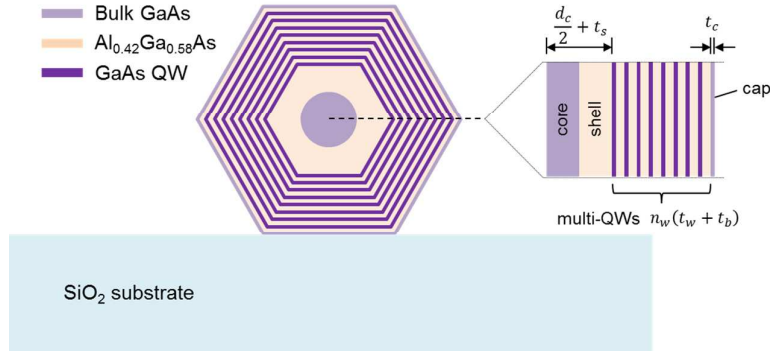


Fig. S1: Schematic showing the cross-section of the GaAs MQW nanowire, with $n_w = 8$ QW tubes, lying on SiO₂ substrate. The diameter of the nanowire is $D = d_c + 2(t_s + n_w t_w + n_w t_b + t_c)$, where d_c is the diameter of the GaAs core, t_s is the thickness of the first AlGaAs layer, t_w is the GaAs QW thickness, t_b is the AlGaAs barrier thickness and t_c is the GaAs cap thickness. The AlGaAs layers have uniform Al concentration of 42%.

To design the lasers, we first model the cavity losses as a function of the nanowire diameter D , in order to identify the diameter and optical mode for which losses are lowest. Once the lowest loss optical mode is identified, we then optimize the position, number and thickness of the MQWs to maximize the modal gain for that particular mode.

a. Modelling cavity losses

As explained in the main text, we first model loss in a GaAs/AlGaAs/GaAs core-shell-cap nanowire. The loss is given by $\alpha_i + \alpha_m$, where α_i is the loss due to absorption in the passive layers (GaAs core and cap) and $\alpha_m = L^{-1} \ln(1/\sqrt{R_1 R_2})$ is the mirror loss, where L is the nanowire length and $R_{1,2}$ are the mode reflectances at the nanowire end facets. For the modelling, we have assumed identical planar end facets for the nanowire laser ($R_1 = R_2$).

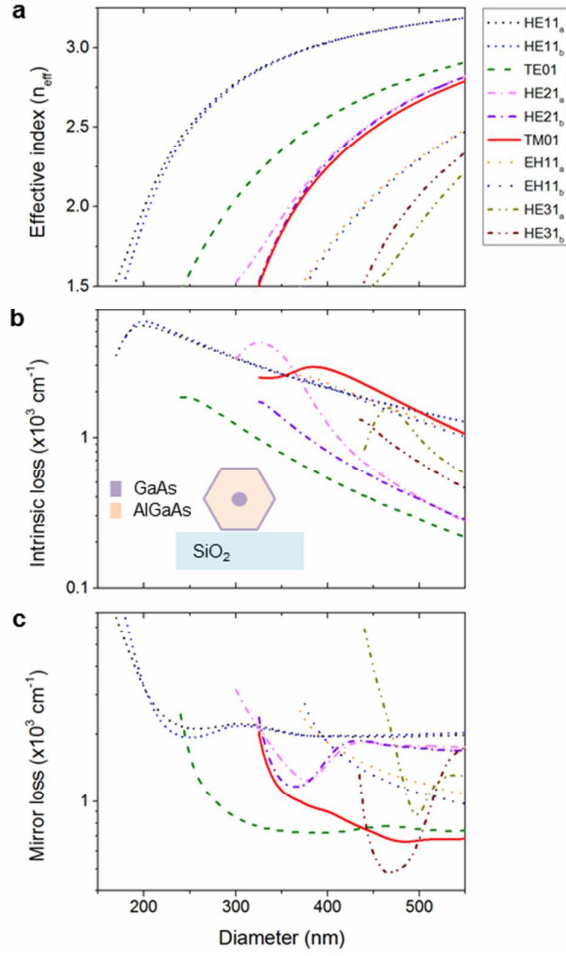


Fig. S2: Effective index (a), mode propagation loss (b) and mirror loss (c) in a GaAs/AlGaAs/GaAs core-shell-cap heterostructure nanowire, as a function of nanowire diameter. The diameter of the core is 80 nm, cap thickness is 5 nm and mode wavelength is 800 nm. The inset in **b** shows the schematic of the nanowire cross-section.

i. Intrinsic loss

Fig. S2a-b shows the mode effective index and mode propagation loss in a GaAs/AlGaAs/GaAs core-shell-cap nanowire, as a function of nanowire diameter. For these calculations, the diameter of the core d_c and the cap thickness t_c were fixed to 80 and 5 nm, respectively, while the AlGaAs shell thickness t_s was varied. The mode free-space wavelength λ_0 was 800 nm. The complex refractive index for SiO₂ and GaAs was taken from Palik¹ and the complex refractive index for Al_{0.42}Ga_{0.58}As was taken from Aspnes². The complex effective index \tilde{n}_{eff} for the guided modes supported in the nanowire was calculated using Lumerical MODE Solutions. The real part of \tilde{n}_{eff} is the mode effective index, shown in Fig. S2a, and the imaginary part of \tilde{n}_{eff} was used to calculate the mode propagation loss, shown in Fig. S2b: $\alpha_i = 2k_0\text{Im}(\tilde{n}_{\text{eff}})$, where $k_0 = 2\pi/\lambda_0$ is the wavenumber. As shown in Fig. S2b, the propagation loss (or intrinsic loss) is the lowest for the TE01 mode across all diameter values. This is because the TE01 mode has a poor overlap with the absorbing GaAs core and cap regions (see Fig. S6a).

ii. Mirror loss

The mode reflectance from nanowire/air interface was calculated numerically using finite-difference time-domain (FDTD) simulations. The FDTD simulation setup and the method to calculate mode reflectance are described in our previous papers^{3,4}. The reflectance was calculated for various modes as function of the nanowire diameter. As above, d_c and t_c were fixed to 80 and 5 nm, respectively, while t_s was varied. We note that only the real part of the complex refractive index was used for the material parameters in these simulations. Fig. S2c shows the mirror loss as a function of the nanowire diameter calculated from the mode reflectance (at $\lambda_0 = 800$ nm) and assuming $L = 5$ μm . The mirror loss is lower at larger diameters and the mode with the lowest mirror loss depends on the nanowire diameter range. These calculations show that for a nanowire laser in which intrinsic loss is negligible, that is $\alpha_i \ll \alpha_m$, different modes can lase depending on the nanowire diameter.

iii. Net modal loss

The net loss in a 5 μm long GaAs/AlGaAs/GaAs core-shell-cap nanowire, with an 80 nm diameter core and 5 nm thick cap, is shown in Figure 1a of the main manuscript and was calculated using the intrinsic and mirror loss shown in Fig. S2b-c, respectively. As discussed in the main manuscript, the TE01 mode has the lowest loss for all diameters above its cut-off diameter (~ 240 nm) and is the best mode for the laser design. The loss for the TE01 mode is presented again in Fig. S3a. For a nanowire with perfect planar end facets, the loss is in the range $1\text{-}2 \times 10^3$ cm^{-1} for diameters between 300-500 nm.

These values provide a lower bound for the estimated modal loss in a GaAs MQW nanowire laser, since perfect planar end facets were assumed. In order to consider the modal loss for a nanowire laser with imperfect end facets, we calculated the loss for the TE01 mode using mode reflectance values that are a factor of 2 and 5 less than those calculated for a perfect planar end facet. The estimated loss for the TE01 mode using these reflectance values is also shown in Fig. S3a. The loss increases to $\sim 4.5 \times 10^3$ cm^{-1} if the end facet reflectance of the TE01 mode is reduced by a factor of 5.

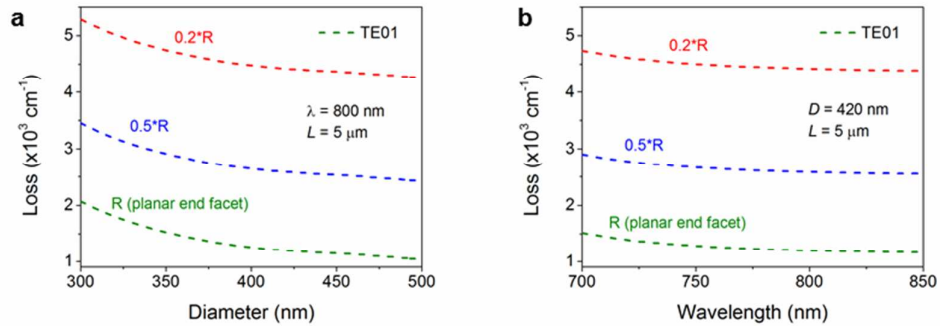


Fig. S3: Loss for the TE01 mode in a 5 μm -long GaAs/AlGaAs/GaAs core-shell-cap nanowire with 80 nm-diameter core and 5 nm-thick cap. **a.** Loss as a function of nanowire diameter at a fixed wavelength of 800 nm. **b.** Loss as a function of wavelength at a fixed diameter of 420 nm. The loss in a nanowire with imperfect end facets with reflectance that is reduced by a factor of 2 (blue) and 5 (red) compared to a perfect planar surface is also shown.

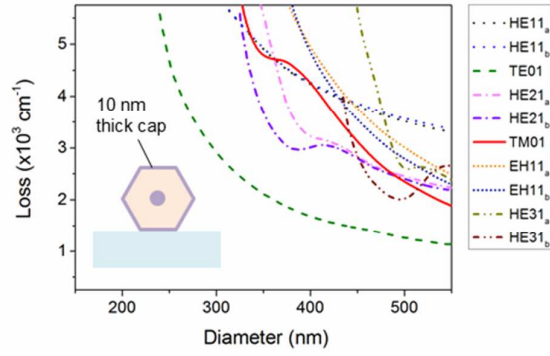


Fig. S4: Modal loss as a function of the nanowire diameter in a GaAs/AlGaAs/GaAs core-shell-cap nanowire with 80 nm-diameter core and 10 nm-thick cap. The nanowire is 5 μm long and the mode wavelength is 800 nm. The inset shows the schematic illustration of the nanowire cross-section.

The calculations were thus far at a fixed wavelength of 800 nm, corresponding to a QW thickness of 4 nm. Fig. S3b shows the loss calculated for the TE01 mode in a 420 nm diameter nanowire as a function of wavelength. The loss does not vary significantly for the range of wavelengths considered because the mode is well confined in the nanowire. The loss is larger at shorter wavelengths due to the larger absorption coefficient in GaAs. Note that the wavelength range of 700-850 nm covers the spectral range of emission from GaAs/ $\text{Al}_{0.42}\text{Ga}_{0.58}\text{As}$ QWs with t_w ranging between 2 to 6 nm. These calculations were used to estimate loss for 2 and 6 nm thick QWs in Figure 1b of main manuscript.

Although the TE01 mode has the lowest loss in our design, the loss for higher order HE modes can be comparable to that for the TE01 mode at large diameters. To suppress mode competition and ensure that large diameter nanowires lase from the TE01 mode, the thickness of the cap can be increased in our design. Fig. S4 shows the modal loss for GaAs/AlGaAs/GaAs core-shell-cap nanowire with a thicker cap (10 nm). All other parameters (d_c , L , λ_0) are the same. The difference in loss between the TE01 mode and the higher order HE modes is much larger in this case compared to when the cap was 5 nm thick (Figure 1a of main manuscript).

In conclusion, the TE01 mode has the lowest loss for a GaAs/AlGaAs/GaAs core-shell-cap nanowire. The losses decrease with increasing nanowire diameter. For the design of the GaAs MQW nanowire laser, we choose a diameter of 420 nm, with 80 nm GaAs core and 5 nm thick GaAs cap. At this diameter, the loss for TE01 mode is small and the difference in losses between the TE01 mode and other modes is large. This diameter is also below the cut-off diameter for the low-loss higher order HE modes.

b. Modelling modal gain

Modal gain is the product of the mode confinement factor and material gain. As discussed in the main text, the modal gain G_m in a laser with QW active regions can be expressed as:

$$G_m = \Gamma_{\parallel} g_{\parallel} + \Gamma_{\perp} g_{\perp} \quad (1)$$

where Γ_{\parallel} and Γ_{\perp} are the mode confinement factors for optical gain parallel g_{\parallel} and perpendicular g_{\perp} to the plane of the quantum well. We will first discuss the material gain modelling for GaAs QWs and then discuss the mode confinement factor calculations.

i. Material gain

In this study we used the material gain calculated for planar GaAs/AlGaAs QWs as an estimate for the material gain of coaxial GaAs/AlGaAs MQWs embedded in our nanowires. We have assumed that the coaxial MQWs have uniform thickness, are uncoupled and are uniformly populated, so that each QW provides equal amount of gain.

We modelled the material gain of planar GaAs/Al_{0.42}Ga_{0.58}As QWs using Simulase, a commercially available software package by Nonlinear Control Strategies⁵. The software uses an $8 \times 8 \mathbf{k} \cdot \mathbf{p}$ model to calculate the single particle wavefunctions and subband energy levels and uses a microscopic many-body gain model to calculate the material gain (www.nlcstr.com/simulase.htm). We calculated the material gain at 300 K for GaAs QWs of thickness 2, 4 and 6 nm. The Al_{0.42}Ga_{0.58}As barriers were 10 nm wide in these calculations and were described by a bulk material model.

The material gain spectrum at three different sheet carrier densities ($4, 6$ and $8 \times 10^{12} \text{ cm}^{-2}$) for electric field polarized in-plane to the QWs (g_{\parallel}) and perpendicular to the plane of the QWs (g_{\perp}) is shown in Fig. S5a-b, respectively. The peak gain of g_{\parallel} is larger than the peak gain of g_{\perp} at these sheet carrier densities, particularly for thinner GaAs QWs (2 nm). The modal gain is thus expected to be larger for modes with electric field polarized in-plane to the QWs.

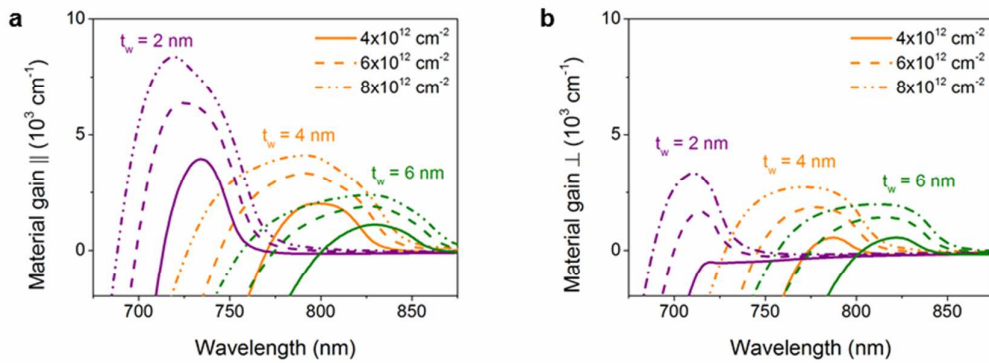


Fig. S5: GaAs/Al_{0.42}Ga_{0.58}As QW material gain spectrum at sheet carrier densities of $4, 6$ and $8 \times 10^{12} \text{ cm}^{-2}$ and QW thickness of 2, 4 and 6 nm. The material gain for TE polarization (electric field parallel to QW plane) and TM polarization (electric field perpendicular to QW plane) is shown in **a** and **b**, respectively.

ii. Mode confinement factor

The mode confinement factor in a nanowire with isotropic gain medium is given by⁶:

$$\Gamma = \frac{c\varepsilon_0 n \iint_{\text{active}} \frac{1}{2} |\mathbf{E}|^2 dx dy}{\iint \frac{1}{2} \text{Re}[\mathbf{E} \times \mathbf{H}^*] \cdot \hat{z} dx dy} \quad (2)$$

where \mathbf{E} and \mathbf{H} are the complex electric and magnetic fields of the guided mode, c is the speed of light in vacuum, ε_0 is the vacuum permittivity, and n is the refractive index of the gain medium. The integral in the numerator is over the active region, whereas the integral in the denominator is across the entire transverse plane of the waveguide. To define the mode confinement factor in a nanowire with coaxial MQWs (as shown in Fig. S1), we first express the numerator in Eqn. 2 in cylindrical polar co-ordinates (ρ, ϕ, z) : $|\mathbf{E}|^2 = |E_\rho|^2 + |E_\phi|^2 + |E_z|^2$. Then if we approximate the coaxial MQWs as cylindrical shells, the E_ϕ and E_z electric field components will be parallel to the QW plane and E_ρ electric field component will be perpendicular to the QW plane. Using this approximation we split the electric field intensity in the numerator into two parts and define Γ_\parallel and Γ_\perp as:

$$\Gamma_\parallel = \frac{c\varepsilon_0 n \iint_{\text{active}} |E_\phi|^2 + |E_z|^2 dx dy}{\iint \text{Re}[\mathbf{E} \times \mathbf{H}^*] \cdot \hat{z} dx dy}, \quad \Gamma_\perp = \frac{c\varepsilon_0 n \iint_{\text{active}} |E_\rho|^2 dx dy}{\iint \text{Re}[\mathbf{E} \times \mathbf{H}^*] \cdot \hat{z} dx dy} \quad (3)$$

Note that $\Gamma = \Gamma_\parallel + \Gamma_\perp$. We will use Eqn. 3 together with Eqn. 1 for calculating the modal gain for all guided modes supported in a 420 nm-diameter nanowire with an 80 nm-GaAs core and 5 nm-thick GaAs cap. However, first we will discuss the mode confinement factor for the TE01 mode.

TE01 mode confinement factor

As shown in Figure 1b of the main manuscript, the electric field of the TE01 mode is polarized azimuthally in the cross-section of the nanowire. Therefore for the TE01 mode, $\Gamma_\perp = 0$ and the modal gain is simply given by $G_m = \Gamma_\parallel g_\parallel$. As discussed in Section I.a, TE01 mode has the lowest loss in our cavity design. To reduce the threshold gain for the TE01 mode, the overlap of TE01 mode with the active region (i.e. Γ for TE01 mode) must be maximized. This can be obtained by proper placement of the QWs in the nanowire and by using multiple QWs.

Fig. S6a shows the electric field intensity profile of the TE01 mode in the cross-section of a nanowire containing a single coaxial GaAs QW. The nanowire heterostructure shown here is identical to that shown in the inset of Figure 1b of the main manuscript. The dimensions of the heterostructure measured in the x-direction are: $D = 420$ nm, $d_c = 80$ nm, $t_s = 83.6$ nm, $t_w = 4$ nm, $t_b = 77.4$ nm and $t_c = 5$ nm. Note that the inner and outer AlGaAs barriers have a uniform thickness of 67 nm when measured along the y-direction; the inner AlGaAs shell is thicker in the x-direction because we have assumed a circular cross-section shape for the core while a hexagonal cross-section shape for the shell.

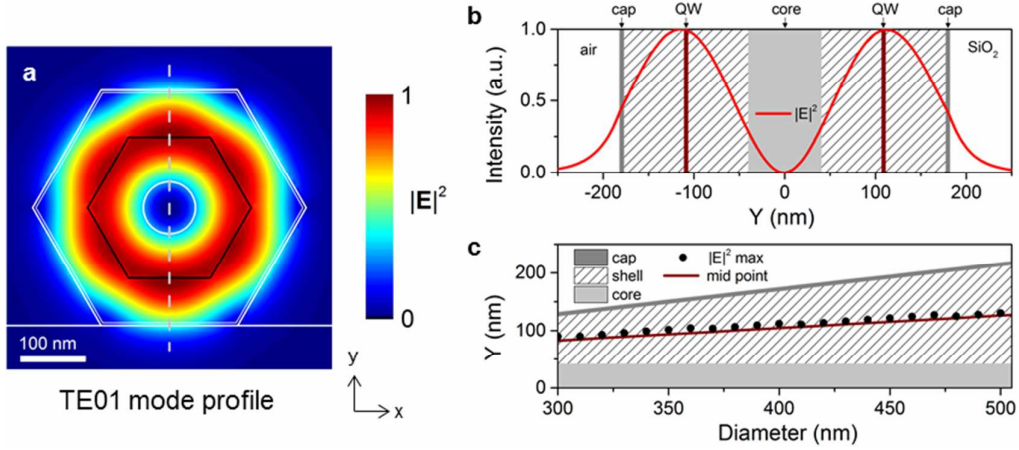


Fig. S6: **a.** Electric field intensity profile of the TE₀₁ mode in a 420 nm-diameter nanowire lying on a SiO₂ substrate. The nanowire has an 80 nm-diameter GaAs core, 83.6 nm-thick AlGaAs shell, 4 nm-thick GaAs QW, 77.4 nm-thick outer AlGaAs shell and 5-nm thick GaAs cap. The mode wavelength is 800 nm. **b.** The mode profile in the nanowire along the dashed grey line shown in **a** (*y*-direction). The position of the QW is close to the field maximum. **c.** The position of the field maximum (back dots) along the *y*-direction in the nanowire, as a function of the nanowire diameter. The field maxima are located approximately at the midpoint of the shell in the nanowire.

As shown in Fig. S6a, the TE₀₁ mode has a doughnut shaped mode profile and the region of maximum intensity coincides well with placement of the coaxial QW. Fig. S6b shows the TE₀₁ mode profile along the *y*-direction in the nanowire. As explained above, the QW is sandwiched between AlGaAs barriers of uniform thickness and is equidistant from the GaAs core and cap. In this heterostructure design, the position of the QW is very close to the peak intensity of the TE₀₁ mode in the nanowire. We find that this design rationale can be used in general for all nanowire diameters. Fig. S6c shows the position of the TE₀₁ mode intensity maximum along the *y*-direction in the nanowire as a function of nanowire diameter. The red line indicates the position that is equidistant from the 80 nm-GaAs core and the 5 nm-thick GaAs cap. The position of maximum intensity is approximately equidistant from the core and cap for all diameters in our design. Thus placing the QW equidistant from the core and cap is an appropriate design rationale to maximize Γ for TE₀₁ mode.

As discussed in the main text, the modal gain from a single QW is insufficient to obtain room-temperature lasing and multiple QWs are required. To design the heterostructure with MQWs, we use the above design rationale and place the MQWs equidistant from the core and cap. For simplicity, the barrier thickness in the *y*-direction t_b^y is assumed to be uniform and is calculated using:

$$t_b^y = \frac{t_s^{total} - n_w t_w^y}{n_w + 1} \quad (4)$$

where n_w is the number of QWs, $t_w^y = \frac{\sqrt{3}}{2} t_w$ is the well thickness in the *y*-direction and t_s^{total} is the total shell layer thickness in the *y*-direction; $t_s^{total} = \frac{\sqrt{3}}{4} D - \frac{\sqrt{3}}{2} t_c - \frac{1}{2} d_c$. In a nanowire with $D = 420$ nm, $d_c = 80$ nm and $t_c = 5$ nm, $t_s^{total} = 137.5$ nm. Note that we obtain $t_b^y = 67$ nm if $n_w = 1$ and $t_w = 4$ nm.

We used Eqn. 4 to design the MQW nanowire heterostructure and calculated the mode profiles using Lumerical MODE Solutions. We then calculated Γ using Eqn. 2 and 3. Table 1 shows the TE01 mode confinement factor in a 420 nm-diameter GaAs MQW nanowire with different QW thicknesses (2, 4 and 6 nm) and different number of QWs (1, 3, 5 and 8). Note that these values were used to calculate the modal gain for TE01 mode shown in Figure 1b of the main manuscript.

As shown in Table 1, the mode confinement factor is proportionate to the QW thickness and the number of QWs, i.e. $\Gamma \propto t_w n_w$. While increasing n_w is advantageous for increasing Γ , care has to be taken to ensure that the barrier thickness t_b^y is large enough for the MQWs to be uncoupled. Note that for $n_w=8$ and $t_w=6$ nm, $t_b^y \sim 10.5$ nm. In planar MQW structures, barrier thicknesses larger than 10 nm are required to avoid coupling.⁷

	$t_w = 2$ nm	$t_w = 4$ nm	$t_w = 6$ nm
$n_w = 1$	0.0244	0.0487	0.0730
$n_w = 3$	0.0605	0.121	0.180
$n_w = 5$	0.0947	0.190	0.276
$n_w = 8$	0.146	0.287	0.426

Table 1: Mode confinement factor for TE01 mode in a 420 nm-diameter nanowire. The GaAs MQW nanowire has 80 nm-diameter GaAs core and 5 nm-GaAs cap. The barrier thickness is uniform along the y-direction and is given by Eqn. 4. The mode wavelength is 730, 800 and 830 nm for the quantum well thickness of 2, 4, and 6 nm, respectively.

iii. Modal gain in a MQW nanowire laser

Modal gain was calculated by multiplying the peak gain of the material gain spectrum with the mode confinement factor, using Eqn.1 and 3. The modal gain for the TE01 mode is shown as a function of sheet carrier density in Figure 1b of the main manuscript. We also calculated modal gain for other guided modes supported in the nanowire. Fig. S7 shows the modal gain for all guided modes supported in a 420 nm-diameter nanowire containing 8 MQWs. The modal gain calculated for 2, 4 and 6 nm-wide MQWs is shown in Fig. S7a-c, respectively. The TE01 mode has the largest modal gain in a nanowire with 2 nm-thick MQWs because $g_{\parallel} > g_{\perp}$. However in thicker QWs or under high injection, g_{\perp} is comparable to g_{\parallel} , and so the modal gain for higher order HE modes, which are fully vectorial and have a good spatial overlap with the coaxial MQWs, can be larger than the modal gain for the TE01 mode.

To assess which mode is likely to lase in our design, we calculated the threshold sheet carrier density from intersection of the loss and gain curves. The horizontal grey lines in Fig. S7a-c are the loss for TE01 mode in a 420 nm-diameter, 5 μm -long nanowire with perfect end facets (see Fig. S3b). We note that the loss for all other modes in this diameter nanowire is larger than $2.5 \times 10^3 \text{ cm}^{-1}$ (see Figure 1a of the main manuscript). The threshold sheet carrier density is clearly the lowest for the TE01 mode in this diameter nanowire and is attainable at room temperature. Thus the TE01 mode is predicted to lase in our design.

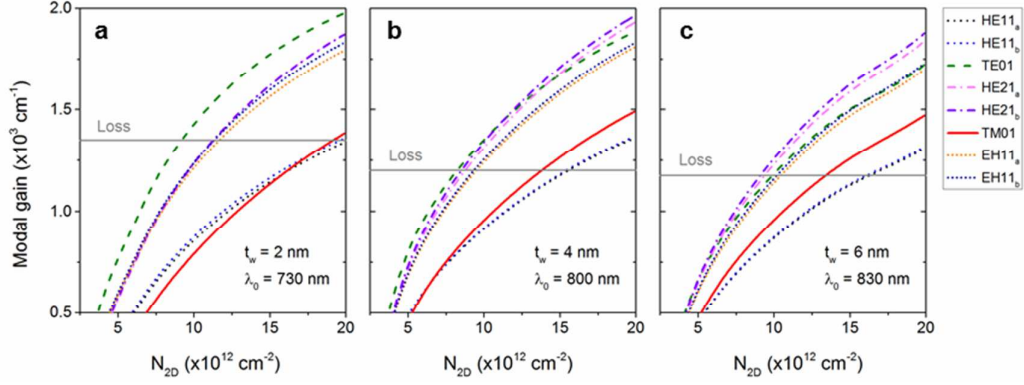


Fig. S7: Estimated modal gain for guided modes supported in a 420 nm-diameter GaAs MQW nanowire (with 8 MQWs) as a function of sheet carrier density. The modal gain for QWs of thickness 2, 4 and 6 nm are shown in **a–c**, respectively. The horizontal grey line is the loss for the TE01 mode.

iv. Optimum number of QWs

Modal gain can also be modelled as a function of current density or pump intensity, for predicting the threshold requirement of electrically driven or optically pumped lasers, respectively. In our experiments, we use a pulsed laser to optically pump the GaAs MQW nanowires. The average carrier density generated in the active region (N_{ave}) can be estimated from the time-averaged pump power (or the pump fluence) used in the experiments (see Eqn. 8 in Section III.e.i). Using Eqn. 8 and assuming that the pump laser spot-size is much larger than the nanowire length, the pump fluence P_f can be expressed as:

$$P_f (\mu\text{Jcm}^{-2}\text{pulse}^{-1}) = \frac{\hbar\omega V_a}{\sigma_{abs}} \cdot N_{ave} \quad (5)$$

where $\hbar\omega$ is the pump photon energy, V_a is the active region volume and σ_{abs} is the nanowire absorption cross-section. Note that V_a is proportional to the QW thickness, the number of QWs and the nanowire length: $V_a \propto t_w n_w L$. Also note that the sheet carrier density N_{2D} is equal to $t_w N_{ave}$ and that for large diameter nanowires, σ_{abs} is proportional to the nanowire diameter and length³: $\sigma_{abs} \propto DL$. Thus for a nanowire with a given diameter, the pump fluence is proportional to the number of QWs and the sheet carrier density: $P_f \propto n_w N_{2D}$.

The above analysis has some important implications for the design of MQW nanowire lasers. Firstly, increasing n_w results in an increase in the pump fluence required to obtain transparency. Secondly, while increasing n_w reduces the threshold sheet carrier density, as shown in Figure 1b of the main manuscript, it may not necessarily reduce the threshold pump fluence required for lasing. This is because the material gain in QWs is a logarithmic function of the carrier density⁸ and so the threshold sheet carrier density does not scale inversely with n_w . Consequently, for a given structure with a certain threshold modal gain (or loss) there exists an optimal n_w to minimize the threshold pump fluence. This result is analogous to the threshold characteristics of planar MQW lasers in terms of the threshold current density⁹.

To determine the optimal n_w for our design, we have calculated the modal gain as a function of the pump fluence using Eqn. 5. The absorption cross-section was estimated from FDTD simulations. Fig. S8a shows the modal gain (at 300 K) for the TE01 mode in a 420 nm-diameter nanowire as a function of pump fluence. The calculations are for 4 nm-thick QWs and show the modal gain with $n_w = 1, 3, 5$ and 8. As discussed above, the pump fluence required for transparency increases with increasing n_w . The loss for the TE01 mode in a 420 nm-diameter nanowire with a cavity length of 5 and 10 μm is also shown in Fig. S8a. The lowest threshold fluence occurs for a nanowire with 8 MQWs. This is also the maximum number of uncoupled QWs that can be placed in a 420 nm-diameter nanowire.

While the design for larger diameter nanowires can possibly accommodate larger number of QWs, simply increasing the number of QWs may not necessarily reduce the threshold pump fluence. To demonstrate this, we have modelled the modal gain vs. pump fluence in a 480 nm-diameter nanowire, as shown in Fig. S8b. The loss for the TE01 mode in a 480 nm-diameter nanowire with a cavity length of 5 and 10 μm is also shown. The lowest threshold fluence is obtained with 8 MQWs for the 5 μm -long nanowire and with 5 MQWs for the 10 μm -long nanowire. Thus, for a given structure with a certain loss (determined by the nanowire diameter and length), there is an optimal n_w to minimise the threshold fluence, which can be determined by using this threshold modal gain/loss modelling approach.

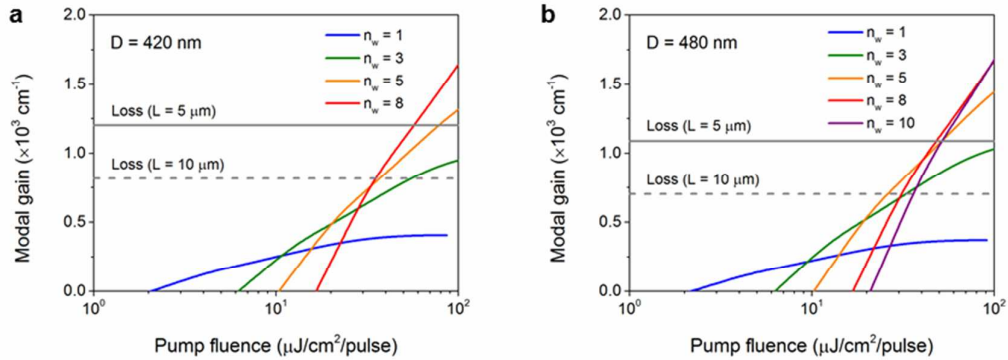


Fig. S8: Modal gain vs. pump fluence for the TE01 mode in a 420 nm-diameter (a) and 480 nm-diameter (b) GaAs MQW nanowire. The GaAs core is 80 nm in diameter and the GaAs cap is 5 nm thick in both a and b. The loss for the TE01 mode in a 5 and 10 μm -long nanowire is also shown in both a and b.

Summary

In summary, we have presented the design for a GaAs MQW nanowire laser. We have optimized the placement of the MQWs in the nanowire to maximize the modal gain for the TE01 mode in a 420 nm-diameter nanowire with 80 nm-GaAs core and 5 nm-thick GaAs cap. We have shown that the TE01 mode has the lowest threshold gain requirement in our design and that 8 is the optimal number of QWs in our design to minimize the threshold pump fluence at room temperature. Our systematic approach to designing the MQW nanowire laser can be applied to optimize the design for MQW nanowire lasers in other cavity configurations and/or in other material systems.

II. Growth and optical characterization

a. Growth of MQW nanowire heterostructure

The growth of the MQW nanowire heterostructure is outlined briefly in the main text. Below, in Table 2, are the details of the growth time used for each shell layer in the heterostructure. As discussed in the main manuscript, the shell growth time for each shell layer was carefully varied in order to ensure that the MQWs were of uniform thickness and that they were positioned correctly in the nanowire, according to the design.

Layer	Time (min:sec)	Layer	Time (min:sec)
AlGaAs0	3:45	QW5	1:52
QW1	1:00	AlGaAs5	4:51
AlGaAs1	3:10	QW6	2:10
QW2	1:10	AlGaAs6	5:33
AlGaAs2	3:31	QW7	2:35
QW3	1:22	AlGaAs7	6:29
AlGaAs3	3:52	QW8	3:02
QW4	1:36	AlGaAs8	7:47
AlGaAs4	4:18	GaAs cap	3:35

Table 2: Growth time for each shell layer in the MQW nanowire heterostructure in chronological order.

b. Structural characterization of nanowires

Fig. S9 shows the SEM image at 57° tilt view of the MQW tube nanowires standing vertically on the growth substrate. The nanowires have a broad tapered base followed by a slightly tapered segment ~ 1.5 μm long and an untapered segment ~ 3.3 μm long. The top part of the nanowires varies across the sample. Some nanowires have regular smooth inclined facets with the 80 nm Au catalyst nanoparticle on top, while others have non-uniform bulky heads. The average diameter of the nanowires (measured at the untapered segment) is 500 nm.

The grown nanowires were sonicated in solution and transferred onto ITO coated glass substrates for optical measurements. We observe that the nanowires usually break off from above the broad tapered base. In some cases the non-uniform bulky head of the nanowires are also broken off during the transfer process (see Fig. S13). The average length of the transferred nanowires was ~ 4.7 μm .

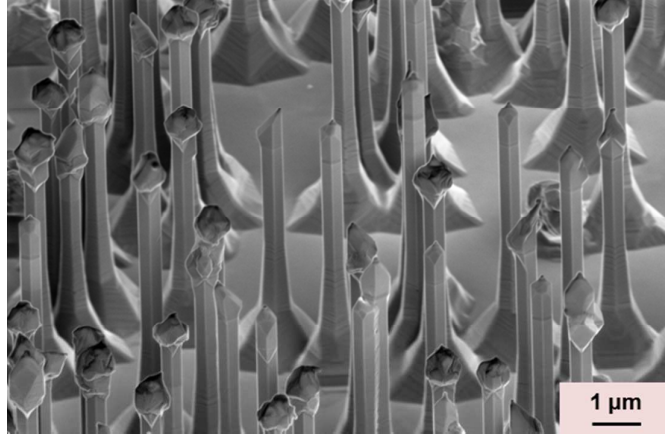


Fig. S9: Scanning electron microscope image of the GaAs MQW nanowires grown for this study. The image is taken at 57° tilt and shows nanowires standing vertically on the growth substrate.

i. Cross-section TEM analysis

The QW and barrier thicknesses were measured from HAADF-STEM images of nanowire cross-sections, including those presented in Figure 2b-c of the main manuscript. Fig. S10a-d shows cross-section images from four other nanowires. The QW/barrier thickness was measured along the $\langle 110 \rangle$ direction, at three different locations, corresponding to the corners (A and C) and middle (B), as indicated in Fig. S10a. Note that the QW thickness varies from one corner to another (A to C). To quantify the thickness, we calculated the average and standard deviation from the measurements. The average QW thickness at positions A-C is 2.5, 3.5 and 5 nm, respectively. The overall average thickness of each layer is shown in Fig. S11. The blue error bars represent the standard deviation of the measurements. As shown in Fig. S11a, the mean thickness of each QW is approximately the same (~ 3.5 nm) and the thickness variation (length of blue error bars) is similar for each QW. As explained in the main text, the thickness variation for each QW is a result of differing growth rates across different crystallographic directions and could not be circumvented in our experiment. However by tailoring the growth time for each QW, we were able to improve the homogeneity between MQWs.

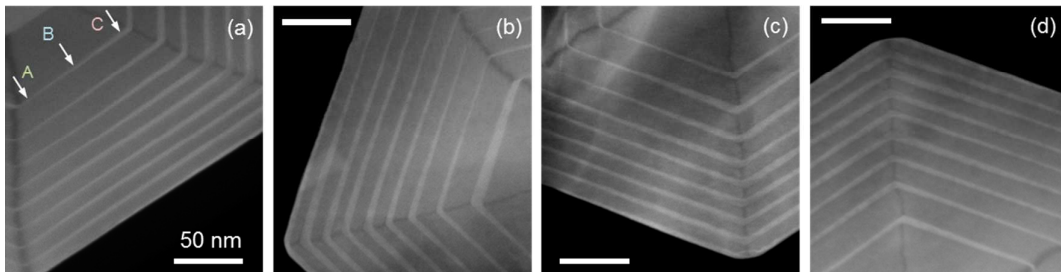


Fig. S10: HAADF-STEM images of nanowire cross-sections. Images **a-d** are from different nanowires. The scale bar is 50 nm. The QW/barrier thicknesses were measured from these images. Each layer was measured at three different positions A-C, as shown in **a**.

The average barrier thickness is shown in Fig. S11b. Note B1 refers to AlGaAs1 in Table 2; the first AlGaAs shell (B0 not shown) has an average thickness of 44.5 nm. As shown in Fig. S11b, barriers 1-3 are thicker than barriers 4-8. The average barrier thickness decreases from B0-B8 and the barriers 4-8 have similar thicknesses (average thickness ranges between 9-10.5 nm).

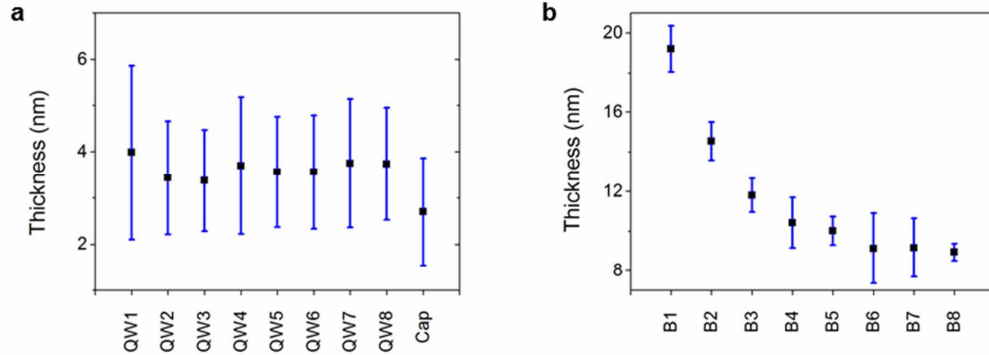


Fig. S11: The average thickness of each layer in the heterostructure, calculated from 5 different nanowire cross-sections. The variation in the thickness is shown by the blue error bars.

c. Photoluminescence measurements

The room temperature photoluminescence (PL) spectrum of a nanowire containing 8 coaxial MQWs is shown in Fig. S12. The spectral data was obtained at very low pump fluence ($\sim 0.01 \mu\text{J}/\text{cm}^2/\text{pulse}$), using a large spot size to excite the entire nanowire. Note that lasing was observed from this nanowire at higher fluence (data presented in Figure 3 of the main manuscript). The PL spectrum from the nanowire exhibits a broad linewidth, which is due to both thermal effects and variations in the QW thicknesses. As described in Ref. 10, the QW thickness and variation in thickness can be characterized by modelling the PL spectrum analytically. We have used this approach to fit the PL spectrum of the MQW nanowire. For the modelling we assumed that the 8 coaxial MQWs were identical, that is the emission energy (or average thickness) and the disorder parameter σ (or thickness variation) of each QW were the same. The analytically derived spectrum, with ground state transition energy of 1.524 eV (vertical dashed line), disorder parameter of 25 meV and electron temperature of 400 K, is shown in Fig. S12. The ground state energy of 1.524 eV is consistent with a QW thickness of ~ 5 nm. Note that for a 5 nm-wide planar GaAs/Al_{0.42}Ga_{0.58}As QW, the ground state energy is 1.536 eV. The other parameter values used for the model are consistent with the values extracted from the PL spectra of nanowires containing a single coaxial GaAs QW, which were grown under the same growth conditions¹⁰.

As shown in Fig. S12, a good fit to the data is obtained using the above parameter values. We note that the discrepancy in the high energy tail is possibly due to the slight variation between QWs, which was not modelled. Nevertheless, the good fit obtained suggests that the MQWs have a high degree of homogeneity and that the broad PL linewidth is largely due to thickness variation of individual QWs.

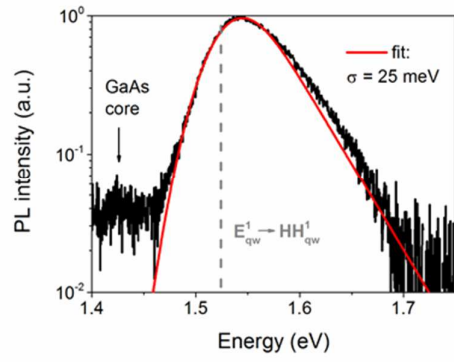


Fig. S12: Room temperature PL spectrum obtained from the GaAs MQW nanowire laser under very low pump fluence and an analytical fit (red line).

III. Laser characterization

a. Nanowire laser dimensions

The nanowire laser dimensions were measured from SEM images. Fig. S13a shows a SEM image of the nanowire lying on an ITO coated glass substrate. The nanowire is 540 nm in diameter and is $4.75 \pm 0.1 \mu\text{m}$ in length. The Au nanoparticle top and tapered base are not present and were broken off during the transfer process for this nanowire. Fig. S13b shows SEM images of the nanowire end facets.

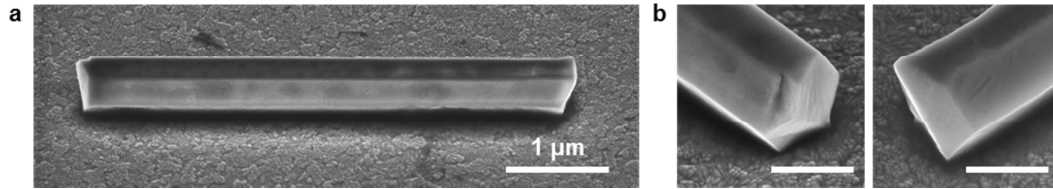


Fig. S13: SEM images of nanowire laser at 45° tilt. **a.** Side view of the nanowire lying horizontally on the ITO coated glass substrate. **b.** Close up view of the nanowire end facets. The scale bar is 400 nm.

b. Lasing spectra

The lasing spectra of the nanowire laser are presented in Figure 3 of the main manuscript. Fig. S14a shows the lasing spectra of the nanowire laser obtained using a fine resolution grating (1200 lines/mm). Note that the emission intensity is graphed on a log scale. Multiple sharp peaks are observed in the lasing spectra, whose intensity is orders of magnitude larger than the background emission level. The multiple peaks observed in the lasing spectra correspond to different axial and transverse modes in the nanowire. We analyzed the spacing of the multiple lasing peaks to calculate the group index (n_g) of the lasing modes, using $\Delta\lambda = \lambda^2/2n_gL$. The dominant lasing peaks in Fig. S14a are regularly spaced ($\Delta\lambda \sim 14 \text{ nm}$) and correspond to a single-transverse-mode with n_g of 4.7 in the nanowire. The subsidiary peaks at shorter wavelengths are spaced closer together and correspond to modes with larger n_g .

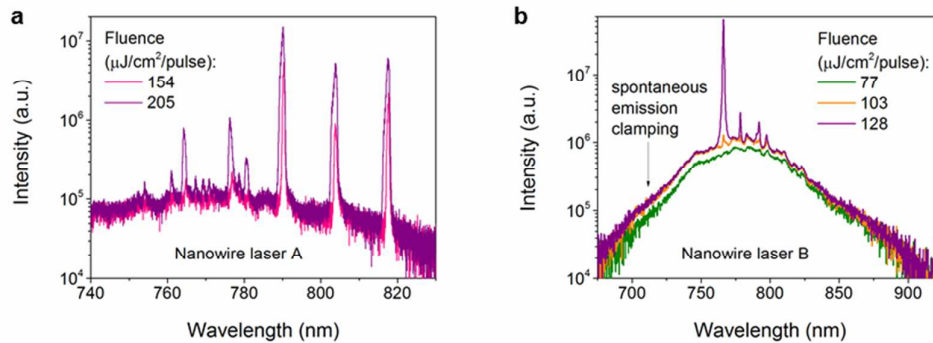


Fig. S14: **a.** The lasing spectra of the nanowire laser presented in the main manuscript, obtained using a fine resolution grating. **b.** The lasing spectra near threshold from a different nanowire to that presented in the main manuscript. Note that the intensity in both **a** and **b** is shown on a log scale.

We also measured the linewidth of the lasing peaks from the spectra by fitting the peaks to a Lorentzian function. At threshold, the peak at 791 nm has a FWHM of ~ 2.5 nm. The Q factor of the cavity, estimated from the linewidth at threshold, is ~ 300 , which corresponds to a threshold modal gain of ~ 1300 cm^{-1} ($\Gamma g_{th} = k_0 n_g / Q$, $k_0 = 2\pi/\lambda$).

While in this manuscript we have analyzed in detail the lasing characteristics from a particular nanowire, we did observe lasing at room temperature from several other nanowires as well in our experiments. Fig. S14b shows the lasing spectra near threshold from a different nanowire to that studied in this manuscript. As shown in Fig. S14b, the transition to lasing is marked by clamping of the background spontaneous emission and dramatic increase in intensity of the lasing mode(s). The threshold fluence for this nanowire was also ~ 110 $\mu\text{J}/\text{cm}^2/\text{pulse}$.

c. Mode confinement factor and group index

The nanowire heterostructure with 8 MQWs was modelled using the average thicknesses measured from the cross-section TEM images (see Fig. S11). The mode profiles were calculated using Lumerical MODE Solutions and the confinement factor was calculated using Eqn. 2 and 3. Fig. S15a shows the TE01 mode profile in the cross-section of the nanowire. The TE01 mode has a good overlap with the inner six MQWs in the nanowire and its mode confinement factor was estimated to be 0.25.

The group index of the guided modes supported in the GaAs MQW nanowire was also calculated using Lumerical MODE Solutions. Fig. S15b shows the group index of the various modes as a function of wavelength. The TE01 mode has a group index of ~ 4.7 , which matches the group index estimated from the spacing of the dominant lasing peaks (Fig. S14a). Since the TE01 mode also has the lowest loss in this diameter nanowire, we attribute the dominant lasing peaks to be from the TE01 mode.

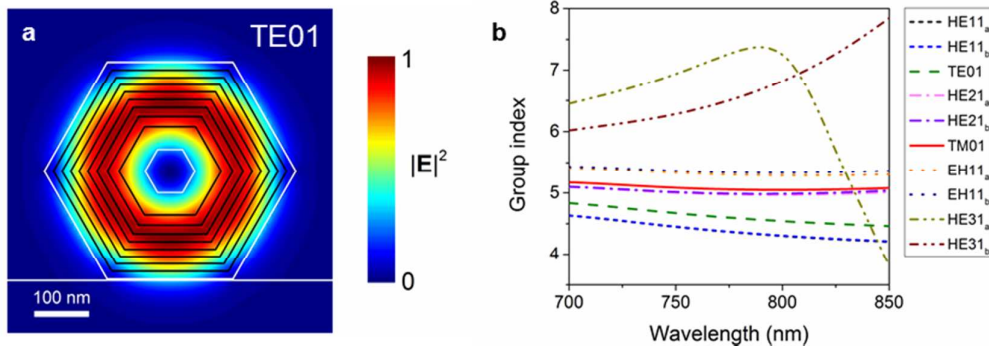


Fig. S15: Simulated TE01 mode profile in the cross-section of the GaAs MQW nanowire. **b.** The group index of the guided modes supported in the nanowire as a function of wavelength.

d. Polarization analysis

The lasing mode was also characterized using polarization measurements. For these measurements, a linear polarizer was placed in front of the spectrometer and spectral measurements were obtained at various polarization angles, with respect to the orientation of the nanowire axis. The integrated spectral emission as a function of polarization angle, below and above threshold, is presented in Figure 3 of the main manuscript. For the data obtained above threshold, only the intensity of the dominant lasing peaks (see Fig. S14a) was integrated. As discussed in the main manuscript, the dominant lasing mode was polarized perpendicular to the nanowire axis and its polarization ratio was estimated to be -0.4.

We also performed FDTD simulations to determine the polarization characteristics of the guided modes supported in the nanowire. In these simulations, guided modes were injected along the nanowire axis and a monitor was placed above the nanowire to record the electromagnetic fields in the near-field. The far-field mode profiles were calculated from the near-field data using plane wave decomposition method.¹¹ For each mode, the polarization of the electric field in the far-field was then resolved at various angles with respect to the nanowire axis⁴ and the far-fields were integrated over a solid angle of 64.15° (since the lens used in experiments had a NA of 0.9). This numerical analysis is comparable with our experiments, in which we analyzed the polarization of emission in the far-field and integrated the spectral emission, as described above.

The polarization characteristics of the guided modes supported in the nanowire laser is presented in Fig. S16. Modes that are polarized perpendicular or parallel to the nanowire axis are shown in Fig. S16a-b, respectively. Although there are several modes that are polarized perpendicular to the nanowire, only the TE₀₁ and HE_{31_b} modes have low threshold modal gain requirements in the nanowire laser, and so are the only modes likely to lase. However the HE_{31_b} mode has a polarization ratio of -0.19, which is smaller in magnitude than the polarization ratio of the dominant lasing mode determined from experiments. Thus, we attribute the dominant lasing mode to be the TE₀₁ mode, which is also consistent with the group index calculations discussed previously.

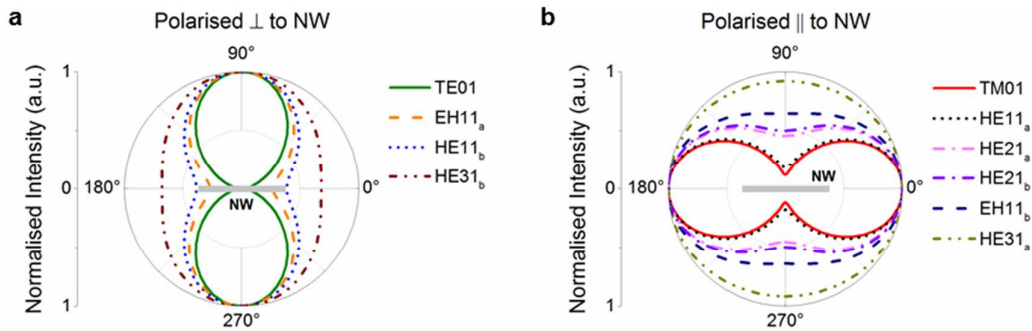


Fig. S16: Polarization dependence of the nanowire guided modes determined from simulations. Modes that are polarized perpendicular or parallel to the nanowire axis are shown in **a** and **b**, respectively.

e. Rate Equation analysis

Rate equations were used to fit the experimental L-L curve and estimate the threshold gain g_{th} and spontaneous emission factor β for the MQW nanowire laser. The rate equations were simplified by making the assumptions that the MQWs have identical thicknesses, are uncoupled, are uniformly pumped and have a uniform carrier density. In addition, we assumed that the multiple lasing modes have the same threshold modal gain, group index and spontaneous emission factor. With these assumptions, the general multimode rate equations^{8,12} were simplified to:

$$\begin{aligned}\frac{dN}{dt} &= \frac{\eta_p P}{\hbar\omega V_a} - \frac{N}{\tau_{nr}} - \frac{N}{\tau_r} - CN^3 - m_s v_g g(N)S \\ \frac{dS}{dt} &= \Gamma v_g (g(N) - g_{th})S + \Gamma\beta \frac{N}{\tau_r}\end{aligned}\quad (6)$$

The first rate equation is for the carrier density N in the active region and the second rate equation is for the average photon density S of the lasing mode in the cavity. The definitions of each of the parameters and the values used to fit the experimental data are provided in Table 3. Here we provide a brief description of some of the parameters.

Optical pump power. The optical pump power P was modelled as a time-dependent function of the form $P_p \operatorname{sech}^2(1.76t/\Delta t)$, where P_p is the peak power of the pulse and $\Delta t = 400$ fs is the pulse width. P_p was calculated from the average power of the pump laser using $P_p \Delta t = P_{ave}/f_p$, where $f_p = 20.8$ MHz is the frequency of the pulsed laser.

Optical pump power absorbed and volume. The fraction of pump power absorbed by the GaAs MQW nanowire was calculated using Lumerical FDTD Solutions. For the simulation, the MQW nanowire heterostructure was modelled using the dimensions measured from SEM and cross-section TEM images. The nanowire volume and the active region volume were also estimated using the measured dimensions. To estimate the carrier density generated in the active region, $\eta_p P/(\hbar\omega V_a)$, we assumed that all carriers absorbed in the barriers were captured into the MQWs.

Recombination rate coefficients. The non-radiative lifetime was estimated from the lifetime extracted from time-resolved PL measurements and was assumed to be a constant. The radiative lifetime however is dependent on the carrier density¹³ and was modelled using Simulase⁵. The radiative lifetime decreases with increasing N and was found to saturate at very large N . The Auger recombination coefficient of bulk GaAs¹⁴ was used as an estimate for the GaAs MQWs.

Material gain. The material gain spectrum of a single planar GaAs/Al_{0.42}Ga_{0.58}As QW was calculated as a function of N using Simulase⁵. The material gain was calculated for a 4 nm-thick QW at a temperature of 350 K (a higher temperature than 300 K was used to account for the expected heating resulting from optical pumping). The peak gain at $\lambda = 800$ nm was then determined from the material gain spectrum and was fitted using the following analytical function:

$$g(N) = \frac{g_0}{1 + \varepsilon N} \ln \left(\frac{N + N_s}{N_{tr} + N_s} \right) \quad (7)$$

The gain model above accounts for gain saturation^{8,15}, which occurs at high carrier densities, as shown in Figure 1b of the main manuscript. The parameters g_0 , N_s , N_{tr} and ε were determined from curve fitting: $g_0 = 3800 \text{ cm}^{-1}$, $N_s = 3.26 \times 10^{18} \text{ cm}^{-3}$, $N_{tr} = 6.5 \times 10^{18} \text{ cm}^{-3}$, $\varepsilon = 1.81 \times 10^{-21} \text{ cm}^3$.

Mode parameters. The group index and mode confinement factor of the TE01 mode was estimated from simulations, as described previously. The threshold modal gain (or cavity loss) for TE01 mode was also estimated from the Q factor calculations.

Table 3: Definition of parameters in rate equations and values used for fit		
Parameter	Definition	Value
η_p	fraction of optical pump power absorbed by active region	10%
$\hbar\omega$	pump laser photon energy	2.375 eV
V_a	volume of the MQW active region	~20% of nanowire volume V $V = 7.5 \times 10^{-13} \text{ cm}^3$
τ_{nr}	non-radiative lifetime (dominated by surface/interface recombination)	5 ns
τ_r	radiative lifetime (dependent on carrier density)	2 ns (for $N > 2 \times 10^{19} \text{ cm}^{-3}$)
C	Auger recombination coefficient	$7 \times 10^{-30} \text{ cm}^6 \text{ s}^{-1}$
m_s	number of lasing modes	3
v_g	group velocity of the lasing mode	c/n_g where $n_g = 4.7$
Γ	mode confinement factor	0.25
g_{th}	threshold gain	5200 cm^{-1}
β	spontaneous emission factor	0.03

i. Comparison between bulk and MQW nanowire lasers

The threshold carrier density in the active region is an important figure of merit for a laser. The average carrier density N_{ave} can be approximated from the time-averaged pump power P_{ave} using:

$$N_{ave} (\text{cm}^{-3}) = \frac{\eta_p A_p}{\hbar\omega V_a} \cdot \left(\frac{P_{ave}}{f_p A_p} \right) \quad (8)$$

where A_p is the pump spot-size area ($\pi d^2/4$ where d is the spot-size). The other terms have been defined previously. Note that the term in parenthesis is the pump fluence. Using Eqn. 8 with the experimentally determined threshold pump fluence of $110 \mu\text{J}/\text{cm}^2/\text{pulse}$ for the GaAs MQW nanowire laser and the parameter values from Table 3, we get $N_{ave} = 3.5 \times 10^{19} \text{ cm}^{-3}$ at threshold.

The threshold carrier density N_{th} can also be determined from modal gain/loss calculations. Modal gain in the GaAs MQW nanowire was modelled using the material gain (at 350 K) and Γ used in the rate equations, and is shown in Fig. S17a as a function of carrier density. The modal loss of 1300 cm^{-1} estimated from the threshold gain ($\Gamma = 0.25$, $g_{th} = 5200 \text{ cm}^{-1}$) is also shown. The intersection of the modal gain and loss curves (blue and black solid lines) gives N_{th} of $3.5 \times 10^{19} \text{ cm}^{-3}$ estimated for the GaAs MQW nanowire laser. Likewise, the threshold fluence P_{th} can be determined from the modal gain/loss curves plotted as a function of pump fluence (using Eqn. 8), as shown in Fig. S17b.

The modal gain/loss calculations enable us to compare the performance of different devices. In Fig. S17 we also present the modal gain/loss for the bulk GaAs nanowire laser that we previously demonstrated.³ The parameters for calculating the modal gain/loss can be found in the Supplementary material of Ref. 3. Coincidentally, the modal loss for this nanowire laser was also estimated to be 1300 cm^{-1} . As shown, N_{th} and P_{th} for the bulk GaAs nanowire laser were $2.5 \times 10^{19} \text{ cm}^{-3}$ and $207 \text{ } \mu\text{J}/\text{cm}^2/\text{pulse}$, respectively.

While N_{th} for the bulk GaAs nanowire laser is $1.4 \times$ smaller than that for the GaAs MQW nanowire laser, P_{th} is $2 \times$ larger. To understand this further, we compared the parameters (V_a , η_p and A_p) for both these devices, which were characterized in the same optical system. V_a of the bulk GaAs nanowire laser was $2 \times$ larger than V_a of the GaAs MQW nanowire laser, while the absorption cross-section ($\eta_p A_p$) was $1.4 \times$ smaller. The larger V_a of the bulk GaAs nanowire laser was found to be the main reason for its larger P_{th} .

The modal gain/loss modelling is also useful for assessing the requirements for further reducing N_{th} and P_{th} for the GaAs MQW nanowire laser. In Fig. S17 we show the modal gain for a GaAs MQW nanowire with $\Gamma = 0.35$ (blue dashed line). We note that a larger Γ could have been realized in our nanowires if the placement of the MQWs could have been further improved. As shown in Fig. S17, increasing Γ for the GaAs MQW laser is predicted to substantially reduce both N_{th} and P_{th} ; both N_{th} and P_{th} are smaller with respect to the previously demonstrated bulk GaAs nanowire laser.

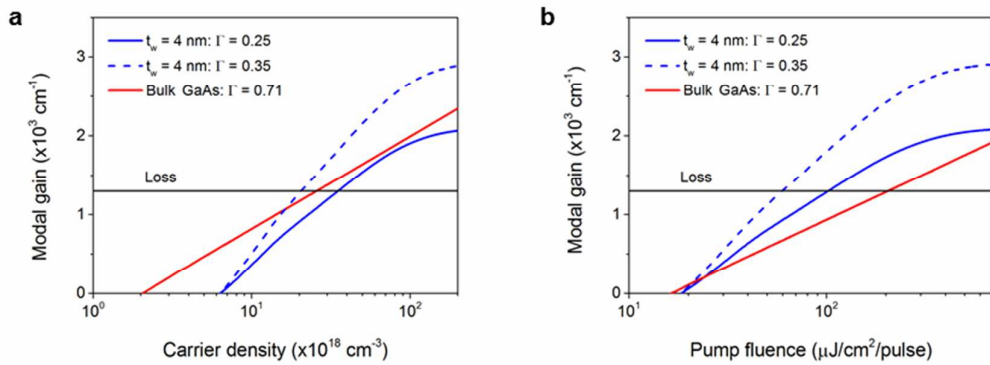


Fig. S17: Modal gain vs carrier density (a) and pump fluence (b) modelled for GaAs MQW (solid blue line) and bulk GaAs (red line) nanowire lasers. The loss of the two lasers is the same and is shown by the horizontal black line. The modal gain for GaAs MQW nanowire with a larger Γ is shown by the dashed blue line.

ii. **Comparison with other reported III-V semiconductor nanowire lasers**

In Table 4 we compare the threshold values of reported III-V semiconductor nanowire lasers. In order to have a fair comparison, we have only included the nanowire lasers that were characterized using femtosecond laser systems (similar to ours). While the threshold fluence is the value mostly reported, the threshold fluence depends on the absorption cross-section, excitation wavelength and active region volume (as described in Eqn. 5). To compare the threshold of nanowire lasers measured with different femtosecond laser systems, we calculated the number of photons per cm^2 at the peak of the pulse (at threshold), using: $N_{ph}^{th} = P_f^{th}/(\hbar\omega\Delta t)$, where P_f^{th} is the threshold pump fluence, $\hbar\omega$ is the pump photon energy and Δt is the pulse width. This value is shown in Table 4 and is clearly lower for the MQW lasers demonstrated in this work, compared to other room-temperature III-V semiconductor nanowire lasers.

Table 4: Comparison of III-V semiconductor nanowire lasers

Reference	Active region material	Threshold fluence* ($\mu\text{J}/\text{cm}^2/\text{pulse}$)	Threshold peak pump-photon intensity (photons/ cm^2)	Threshold gain (cm^{-1})	Threshold time-averaged carrier density (cm^{-3})
This work	GaAs/AlGaAs MQWs	110 at RT	7.2×10^{26}	5200	3.5×10^{19}
Stettner et al. ¹⁶	GaAs/AlGaAs MQWs	30-67 at 19 K	$0.5\text{-}1.0 \times 10^{27}$	-	-
Tatebayashi et al. ¹⁷	InGaAs/GaAs QDs	~ 200 at RT	3.9×10^{27}	140,000	-
<i>Bulk active region – nanowire lying horizontally on dielectric substrate</i>					
Chin et al. ¹⁸	GaSb	~ 50 at 30 K	1.4×10^{27}	-	$\sim 4 \times 10^{18}$
Mayer et al. ¹⁹	GaAs/AlGaAs bulk	~ 204 at RT	5.3×10^{27}	-	-
Saxena et al. ³	GaAs/AlGaAs bulk	~ 207 at RT	1.4×10^{27}	1800	2.5×10^{19}
Burgess et al. ²⁰	p-doped GaAs bulk	~ 200 at RT	1.3×10^{27}	1300	$\sim 2 \times 10^{19}$
Gao et al. ²¹	InP bulk	~ 130 at RT	8.5×10^{26}	-	-
<i>Bulk active region – nanowire standing vertically on substrate</i>					
Chen et al. ²²	InGaAs/GaAs bulk	~ 100 at RT	3.1×10^{27}	1400	-
Sun et al. ²³	InGaAs/InGaP bulk	~ 40 at RT	1.3×10^{27}	-	-
Mayer et al. ²⁴	GaAs/AlGaAs bulk	~ 17 at 10 K	1.5×10^{26}	-	-

*So that the threshold values are comparable, only those nanowire lasers that were characterized using femtosecond laser systems (pulse width 150 – 450 fs) are compared.

The threshold carrier density is however the best figure of merit to compare different nanowire lasers, with different active regions and cavity configurations. Unfortunately, the threshold carrier density of nanowire lasers is not often reported. The threshold gain is also useful for comparing nanowire lasers of different dimensions; however this too is not often reported. The threshold gain and threshold carrier density that have been reported are provided in Table 4. The threshold gain for the MQW laser is larger than that for bulk nanowire lasers because of its smaller Γ (smaller mode overlap with the active region). As described in the previous section, improving the mode overlap (increasing Γ from 0.25 to 0.35) in our nanowires is predicted to significantly reduce both the threshold carrier density and threshold fluence. In particular, the threshold carrier density of the optimized structure is predicted to be much lower compared to nanowire lasers with bulk active region.

Finally, we note that the nanowire lasers demonstrated in this work have lower thresholds than other III-V semiconductor QW/QD nanowire lasers reported^{16, 17}. Also, lasing is observed from the ground state of the quantum confined active region, unlike the reported QD nanowire lasers¹⁷ which lase at room-temperature from excited states.

IV. References

- 1 Palik, E. D. *Handbook of Optical Constants of Solids*. (Academic Press, 1998).
- 2 Aspnes, D. E., Kelso, S. M., Logan, R. A. & Bhat, R. Optical properties of Al_xGa_{1-x}As. *J. Appl. Phys.* **60**, 754-767 (1986).
- 3 Saxena, D. *et al.* Optically pumped room-temperature GaAs nanowire lasers. *Nat Photon* **7**, 963-968 (2013).
- 4 Saxena, D. *et al.* Mode Profiling of Semiconductor Nanowire Lasers. *Nano Letters* **15**, 5342-5348 (2015).
- 5 Nonlinear Control Strategies. <<http://www.nlctr.com/>> (2016).
- 6 Ning, C. Z. Semiconductor nanolasers. *physica status solidi (b)* **247**, 774-788 (2010).
- 7 Harrison, P. *Quantum Wells, Wires and Dots: Theoretical and Computational Physics*. (John Wiley & Sons, 2000).
- 8 Coldren, L. A., Corzine, S. W. & Masanovic, M. L. *Diode lasers and photonic integrated circuits*. Second edn, 157-256 (Wiley, 2012).
- 9 Arakawa, Y. & Yariv, A. Quantum well lasers--Gain, spectra, dynamics. *Quantum Electronics, IEEE Journal of* **22**, 1887-1899, doi:10.1109/jqe.1986.1073185 (1986).
- 10 Davies, C. L. *et al.* Low ensemble disorder in quantum well tube nanowires. *Nanoscale* **7**, 20531-20538 (2015).
- 11 Lumerical Solutions. <https://kb.lumerical.com/en/index.html?solvers_far_field_projections.html> (2016).
- 12 Chang, S.-W., Lin, T.-R. & Chuang, S. L. Theory of Plasmonic Fabry-Perot Nanolasers. *Opt. Express* **18**, 15039-15053 (2010).
- 13 Bishop, P. J., Daniels, M. E., Ridley, B. K. & Woodbridge, K. Radiative recombination in GaAs/AlGaAs quantum wells. *Physical Review B* **45**, 6686-6691 (1992).
- 14 Strauss, U., Ruhle, W. W. & Kohler, K. Auger recombination in intrinsic GaAs. *Applied Physics Letters* **62**, 55-57 (1993).
- 15 Chuang, S. L. *Physics of Optoelectronic Devices*. 337-402; 487-493 (Wiley, 1995).
- 16 Stettner, T. *et al.* Coaxial GaAs-AlGaAs core-multishell nanowire lasers with epitaxial gain control. *Applied Physics Letters* **108**, 011108 (2016).
- 17 Tatebayashi, J. *et al.* Room-temperature lasing in a single nanowire with quantum dots. *Nat Photon* **9**, 501-505 (2015).
- 18 Chin, A. H. *et al.* Near-infrared semiconductor subwavelength-wire lasers. *Applied Physics Letters* **88**, 163115-163113 (2006).
- 19 Mayer, B. *et al.* Lasing from individual GaAs-AlGaAs core-shell nanowires up to room temperature. *Nat Commun* **4**, (2013).
- 20 Burgess, T. *et al.* Doping-enhanced radiative efficiency enables lasing in unpassivated GaAs nanowires. *Nat Commun* **7**, (2016).
- 21 Gao, Q. *et al.* Selective-Area Epitaxy of Pure Wurtzite InP Nanowires: High Quantum Efficiency and Room-Temperature Lasing. *Nano Letters* **14**, 5206-5211 (2014).
- 22 Chen, R. *et al.* Nanolasers grown on silicon. *Nat Photon* **5**, 170-175 (2011).
- 23 Sun, H. *et al.* Nanopillar Lasers Directly Grown on Silicon with Heterostructure Surface Passivation. *ACS Nano* **8**, 6833-6839 (2014).
- 24 Mayer, B. *et al.* Monolithically Integrated High- β Nanowire Lasers on Silicon. *Nano Letters* **16**, 152-156 (2016).